Geophysical Journal International

Geophys. J. Int. (2015) **203,** 541–547
GJI Seismology

doi: 10.1093/gji/ggv314

Oceanic crust in the mid-mantle beneath west-central Pacific subduction zones: evidence from *S* to *P* converted waveforms

Zhongtao Yang and Xiaobo He

Department of Marine Sciences, Ocean College, Zhejiang University, Zhousan, Zhejiang, China. E-mail: xbhe@zju.edu.cn

Accepted 2015 July 24. Received 2015 July 24; in original form 2015 May 7

SUMMARY

The fate of subducted slabs is enigmatic, yet intriguing. We analyse seismic arrivals at ∼20–50 s after the direct *P* wave in an array in northeast China (NECESSArray) recordings of four deep earthquakes occurring beneath the west-central Pacific subduction zones (from the eastern Indonesia to Tonga region). We employ the array analysing techniques of fourth root vespagram and beam-forming analysis to constrain the slowness and backazimuth of later arrivals. Our analyses reveal that these arrivals have a slightly lower slowness value than the direct *P* wave and the backazimuth deviates slightly from the great circle direction. Along with calculation of 1-D synthetic seismograms, we conclude that the later arrival is corresponding to an energy of *S*-to-*P* converted at a scatterer below the sources. Total five scatterers are detected at depths varying from ∼700 to 1110 km in the study region. The past subducted oceanic crust most likely accounts for the seismic scatterers trapped in the mid-mantle beneath the west-central subduction zones. Our observation in turn reflects that oceanic crust at least partly separated from subducted oceanic lithosphere and may be trapped substantially in the mid-mantle surrounding subduction zones, in particular in the western Pacific subduction zones.

Key words: Composition of the oceanic crust; Body waves; Subduction zone processes; Pacific Ocean.

1 INTRODUCTION

The fate of subducted slabs is a key ingredient in the theory of plate tectonics (Wen & Anderson 1995). In the upper mantle, the slabs can be configured by deep earthquakes surrounding subduction zones (e.g. Gudmundsson & Sambridge 1998); however, due to an absence of very deep seismicity, there is no direct evidence to conclude the fate of subducted slabs at depths below 670 km. Current understanding mostly comes from seismic tomography (e.g. Grand 2002; Fukao & Obayashi 2013), but which is limited in resolution, especially for deep mantle structures.

Evidences from analyses of the coda and precursors of seismic phases (e.g. PKP, PKKP, PP, Pdiff, etc.) indicate strong small-scale heterogeneity (i.e. scatterers) in the mantle at depths greater than 660 km (e.g. Hedlin *et al.* 1997; Niu & Wen 2001; Hedlin & Shearer 2002; Bentham & Rost 2014). The small-scale deep mantle structure exhibits a localized distribution and has been suspected to be associated with remnants of subducted slabs at various depths (e.g. Helffrich & Wood 2001; Shang *et al.* 2014); nevertheless, this conclusion still suffers from a lack of direct seismic observations. Therefore, it is necessary to find direct evidences to correlate subducted slabs with fast seismic anomalies at great depths, especially for the small-scale structures associated with crustal component of subducted slabs.

Seismic discontinuities at mid-mantle depths, between 670 and 1800 km depths, have been identified along the western Pacific subduction zones from *S*-to-*P* converted waves below deep seismic sources (e.g. Kawakatsu & Niu 1994; Castle & Creager 1999; Kaneshima & Helffrich 1999; Krüger *et al.* 2001; Castle & van der Hilst 2003; Vanacore *et al.* 2006; Zhou *et al.* 2012; Li & Yuen 2014). This mid-mantle seismic discontinuity has been further interpreted as a distinct compositional layer most likely associated with subducted oceanic crust (Niu 2014). This converted seismic energy probably provides the most direct signal to reflect the small-scale structure in the deep mantle.

In this study, we aim to perform a systematic search for deep mantle small-scale structures beneath the west-central Pacific subduction zones (the eastern Indonesia, Solomon area and Tonga region) by using the recently released array data in northeast China (NECESSArray). The conventional array analysing techniques (fourth root vespagram and beam-forming analysis; Rost & Thomas 2002) are applied to constrain the slowness of observed *S*-to-*P* arrivals. The mid-mantle discontinuities have been detected beneath the eastern Indonesia (Vanacore *et al.* 2006) and Tonga region (e.g. Zang *et al.* 2006; Kaneshima 2009, 2013), but have not been revealed beneath the Solomon region. Therefore, the primary goal of this study is to demonstrate if these small-scale structures are ubiquitously present in the mid-mantle (depth from 670 to 1800 km) beneath the

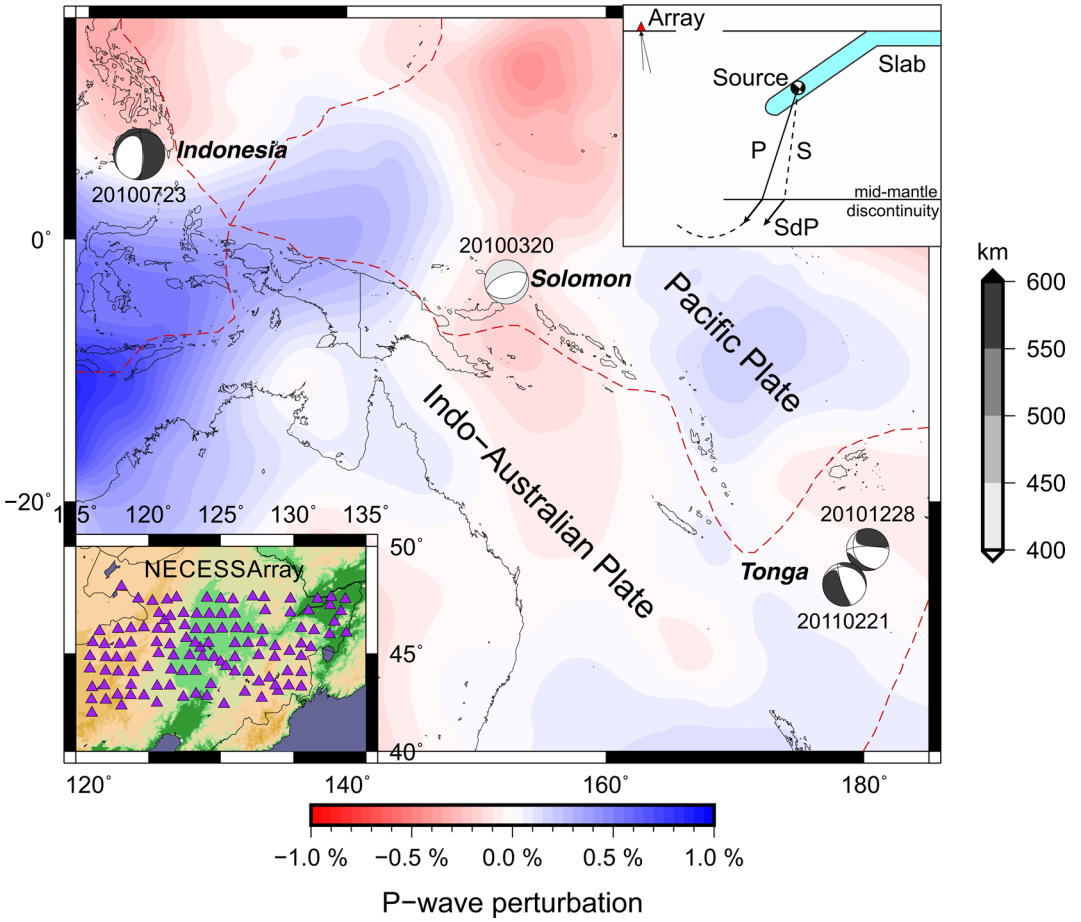

Figure 1. Location of the four events (see Table 1 for details) used and the station distributions of NECESSArray. The *P* velocity model (Fukao & Obayashi 2013) for the depth range 991–1095 km is shown in the background. Top right insert is a schematic plot depicting the geometric ray paths for both of *P* and *SdP*.

west-central Pacific subduction zones. Along with previous publications, we can suspect whether it is ubiquitous beneath the whole subduction zones. Based on our observations, some implications on mantle dynamics, plate tectonics and mantle heterogeneity as well as deep water cycle are also discussed.

2 DATA AND ANALYSIS

We study four events occurring from 2010 to 2011 with depths greater than ∼400 km beneath the west-central Pacific subduction zones (one event in the eastern Indonesia, one event from the Solomon area and two events in the Tonga region; Fig. 1 and Table 1). The great circle paths linking the events to the NECESSArray along with the piercing points of later arrivals at the mid-mantle discontinuities below sources are presented in Fig. S1 of the Supporting Information. Broad-band seismic waveform data in vertical component from the NECESSArray are collected. We apply a 2-pass, 2-pole Butterworth bandpass filter with corner frequencies at 0.1 and 1 Hz to the data. We analyse the *S*-to-*P* conversion wave, which starts as a down-going *S* wave and is subsequently converted to a *P* wave at the mid-mantle discontinuity or scatterer below sources. Therefore, *S*-to-*P* phase displays a nearly identical (slightly lower) slowness compared to direct *P*, which helps to identify the conversional wave in the vespagram. The array analysing technique (fourth root vespagram; Rost & Thomas 2002) is applied to enhance the coherent signals and constrain their slowness for phase identification and estimation of conversion depth based on a slightly modified IASP91 model (Kennett & Engdahl 1991) by incorporating a seismic low-velocity layer below sources. The heterogeneous local structure will generate waves that propagate out of the great circle path. The beam-forming analysis is used to jointly constrain the slowness and backazimuth of later arrivals. The constrained backazimuth is slightly different from the great circle direction for all the data used in this study (Fig. 2). For comparison, the beam-forming analyses of direct *P* are also presented in Fig. S2 of the Supporting Information. The synthetic seismograms are produced to further understand the nature of later arrivals as well as the seismic property of scatterers below sources, which are responsible for generating the later arriving signals (Fig. 3). Niu *et al.* (2003) suggested that V_s and density within the scatterer are, respectively, 2–6 per cent lower and 2–9 per cent higher than those of the ambient mid-mantle. No significant change in V_p between the scatterer

Table 1. Earthquakes used in the study and observations of the *SdP*.

Event date	Lat.	Lon.	Event depth (km)	Mag. (M_w)	*SdP* conversion depth (km)
2010–03–20	152.28E	3.38S	418.9	6.6	700
2010–07–23	123.58E	6.42N	584.7	7.7	910
2010–12–28	179.72W	23.41S	550.9	6.3	780
2011–02–21	178.48E	26.04S	551.8	6.5	880, 1110

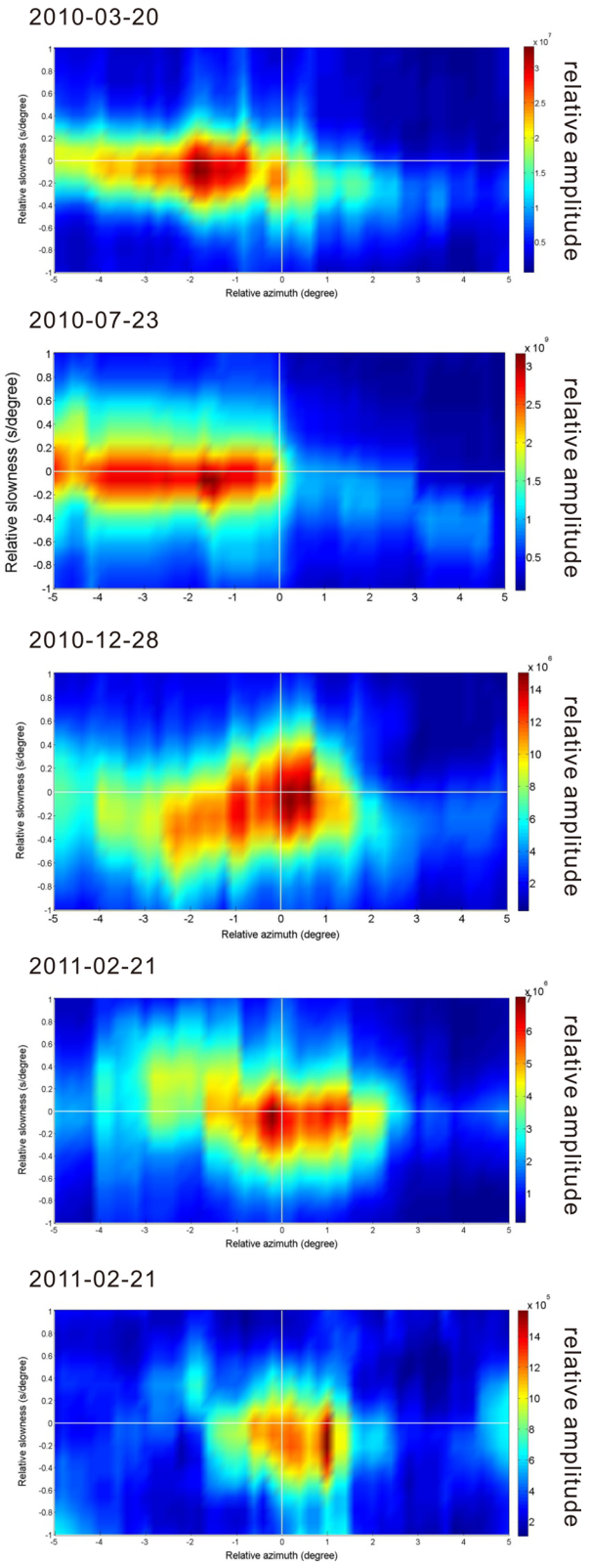

Figure 2. Beam-forming analysis for four events data used in this study shows the later arrival's slowness relative to the one of *P* wave and backazimuth relative to the great circle. Overall, the *SdP* incoming direction is less than 2° away from the backazimuth defined by the source and receiver. The accuracy of slowness and azimuth tightly relies on the coherency of *SdP* arrivals.

and the surrounding mantle occurs. This observation is compatible with the predicted elastic properties of oceanic crust in the mid-mantle (Tsuchiya 2011). And accordingly, here a slightly modified Iasp91 model is introduced for the calculation. A 7 km thick low-velocity (velocity and density change by −4 per cent and 5 per cent, respectively) layer is constructed and placed below the sources in the model (Niu 2014). The corresponding fourth root vespagrams for the synthetic sections are also calculated to compare with the data.

We plot record sections to show the major arrivals (e.g. *P*, *pP*, etc.) and their coda. All the seismograms are aligned along the direct *P* wave. Here, we present the record section and the vespagram for the 2010 March 20 event (see Table 1 for details) as an example to describe the data processing (Fig. 3). We calculate the fourth root vespagram by varying the slowness between −1 and 1 s deg^{-1} with an increment of 0.1 s deg^{-1}. Record sections for other three events, along with their vespagrams, are presented in the Supporting Information (see Figs S3–S5). The record sections for four events show clear arrivals at ∼20–50 s after the direct *P* wave that is not predicted by the IASP91 model (Kennett & Engdahl 1991). They are mostly visible even without enhancing processing. The constrained slowness of later arrivals exhibit slightly lower values than those of direct P, suggesting that these arrivals are most likely an *S* to *P* converted phase from a localized structure below the sources (e.g. Kawakatsu & Niu 1994; Kaneshima & Helffrich 1999; Krüger *et al.* 2001; Kaneshima 2003; Niu *et al.* 2003; Zhou *et al.* 2012). A dipping structure below sources significantly boosts the energy of *S*-to-*P* wave, making *SdP* being prominent (Niu 2014). Hence, the discrepancy in amplitude between observed and synthetic *SdP* arrivals can be partly attributed to a dipping structure (Fig. 3c and Figs S3–S5c in the Supporting Information). The fact is that there is a trade-off between the dipping structure and seismic contrast. It is still a challenge to isolate one from them without *a priori* knowledge. In this study, we only consider a flat low-velocity layer placed below the source suggested by previous studies (Niu *et al.* 2003; Niu 2014). Future 3-D modelling is needed to further understand the geometric structure of seismic scatterers in the mid-mantle.

3 RESULTS

Fourth root vespagrams of the four events analysed exhibit a mid-mantle discontinuity ranging from ∼700 to 1110 km throughout the study region. Total five scatterers are detected from our data analyses. Particularly, two scatterers below sources are detected only by one event recording (Fig. S5, Supporting Information) in Tonga region. The constrained depths of mid-mantle discontinuity (i.e. *SdP* conversion depth) in this study are summarized in Table 1. Here, we elaborate our observations from north to south along the study region.

3.1 The eastern Indonesia

A mid-mantle discontinuity at a depth of ∼910 km is revealed by analysing the recording of the 2010 July 23 event in the eastern Indonesia (Fig. S3, Supporting Information). The seismic scatterer deviates from the great circle direction by ∼1.7° (Fig. 2). The estimated depth is close to the previous constraints of ∼930 and 970 km in the same area (Vanacore *et al.* 2006). The varied depth is either due to analysed seismic signals produced from three isolated scatterers, or one giant structure with the seismic waves sampling

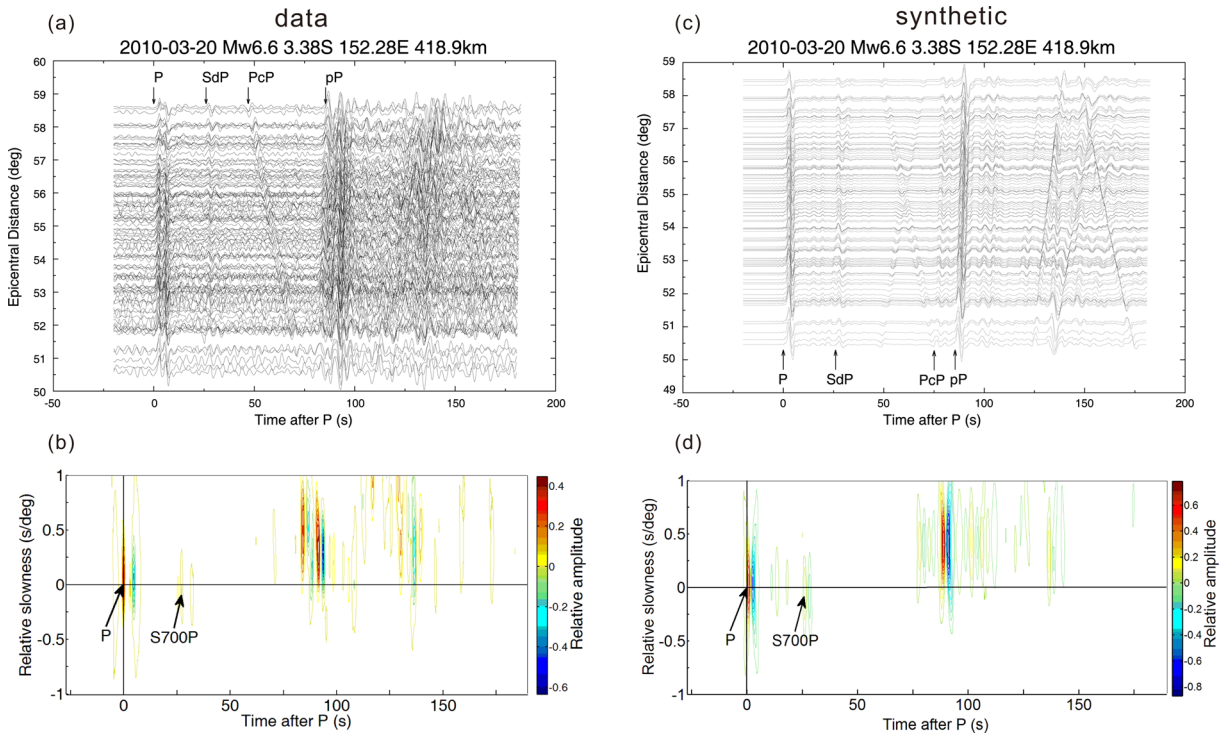

Figure 3. (a) The seismic record section and (b) fourth root vespagram for the 2010 March 20 event. (c) The corresponding synthetic traces computed in a modified IASP91 model and (d) its vespagram. A scatterer at ∼700 km depth below the source is detected in the Solomon area. We vary the slowness between −1 and 1 s deg^{-1} with an increment of 0.1 s deg^{-1} to produce the vespagram. A pronounced later arrival exhibits a slightly negative slowness compared to the *P* wave. They can be seen in most of individual traces. The modified iasp91 model (a low-velocity layer is placed at ∼700 km depth) was employed to generate the synthetic traces via the propagation matrix method. The direct *P*, depth phase *pP*, core-reflected phase *PcP* and *SdP* are well reproduced by synthetic calculation. Note that a clear phase, perhaps associated with the upper-mantle discontinuities, ahead of *pP* is shown in the synthetic section.

different portion of the structure. Future investigations with migration techniques are preferred to image the small-scale structures in great details. The structure may be a fragment of subducted slab between 45 and 25 Ma beneath the Philippines-Halmahera arc north of Australia (Hall 2002).

3.2 The Solomon area

In the Solomon area, a scatterer at a depth of ∼700 km is detected from analyses of the 2010 March 20 event data (Fig. 3). The beam-forming analysis reveals that the backazimuth of the S700P is approximately 1.9° away from the great circle path defined by the source and receiver (Fig. 2). To our knowledge, this is the first report of a small-scale structure at mid-mantle depth in this place. The scatterer appears to be well correlated with the location of the high-velocity anomalies in a regional tomographic model (Hall & Spakman 2002). This tomographic anomaly has an NNE–SSW trend and can be seen up to the depth of ∼1100 km, suggesting a remnant of Cretaceous subduction (Hall & Spakman 2002).

3.3 The Tonga region

Three small-scale structures below two sources are revealed at depths ranging from ∼780 to 1110 km in the Tonga region (Figs S4–S5, Supporting Information). A seismic discontinuity at a depth of about 920 km in the mantle has been revealed beneath the Tonga subduction zone (Kawakatsu & Niu 1994). Subsequent investigations have revealed multiple discontinuities present at ∼600–1000 km depth by analysing *SdP* phases (Zang *et al.* 2006) and seismic scatterers trapped at the shallowest lower mantle in this region from studies of *S*-to-*P* scattered waves (Kaneshima 2009, 2013). All the observations together suggest a complex mid-mantle structure beneath the Tonga subduction zone. This complication characteristic is in agreement with the signature revealed by studies of the deep seismicity (e.g. Brudzinski & Chen 2005; Bonnardot *et al.* 2009) as well as the *P* tomographic images of the subducted slabs surrounding this region (van der Hilst 1995; Fukao & Obayashi 2013).

4 DISCUSSION

4.1 *S*-to-*P* conversion or *P*-to-*P* reflection

The observed seismic features of later arrivals here are very similar to those of the *S*-to-*P* converted waves that have been identified in other subduction zones (e.g. Vanacore *et al.* 2006; Li & Yuen 2014). Specifically, the slowness of later arrivals is slightly lower than that of *P* wave, and the delay time between the later arrival and *P* wave can be up to 50 s. Such a huge delay is difficult to explain without an *S* segment involved along the ray path because *S* wave travels slower than *P* wave does. To consider this interpretation further, a synthetic section has been produced after filtering the down-going *SV* waves by propagation matrix approach (Wang 1999) for the 2010 March 20 event (Fig. S6, Supporting Information). The synthetics clearly demonstrate that the later arrival has been removed after applied filtering. And accordingly, the signal is concluded to be *S*-to-*P* conversion at deep scatterers, rather than *P*-to-*P* reflection.

4.2 Low-velocity layer and discontinuity

The *S*-to-*P* conversion signal has been suspected to result from a dipping low-velocity layer other than a sharp seismic discontinuity resulting from a phase change in the mid-mantle (Niu 2014). If the conversion occurs at a sharp discontinuity, then a ∼10 per cent increase in V_s is required to explain the amplitude of an *S*-to-*P* arrival. Such a large velocity drop due to a phase change has been rarely reported in the mid-mantle (Niu 2014). In addition, a phase change discontinuity generally exhibits flat globally with a few kilometres fluctuation, whereas the discontinuity presented here ranges in various depths (∼700 to 1110 km). Therefore, we prefer a low-velocity layer to explain the *SdP* arrival.

4.3 The seismic property of low-velocity layer

Although there exists discrepancy in amplitude of *SdP* between data and synthetics, but the waveform modelling successfully predicts the arrival time and slowness of *SdP*. The 7 km thick layer in the model for simulation is also compatible with the structure resolved by a signal with dominant frequency (0.1–1 Hz). The seismic structure observed here appears to be very similar to the dipping structures observed by previous studies (Niu *et al.* 2003; Niu 2014). The local structures are speculated to have higher density, lower V_s and no significant V_p anomaly when compared to the ambient mantle. The signatures excellently agree with results from a recent mineral physics calculation of elasticity of oceanic crust with a MORB composition (Tsuchiya 2011). All the observations together suggest that the observed structure is likely a fragment of former subducted oceanic crust. This indication is well consistent with the recent suggestion from study of PP and its precursors generated from scatterers beneath western Pacific subduction zones (Bentham & Rost 2014). However, we are still suffering from a lack of robust mineral physics data on the seismic properties of MORB in the mid-mantle condition. And accordingly, it is a challenge to directly link the seismic observations with the mineral physics data. In the future, a multidisciplinary approach is necessary to improve our understanding of seismic property in the mid-mantle.

4.4 The separated oceanic crust or the whole slab

To understand if the oceanic crust observed in the mid-mantle has separated from or attached to the main subducting lithosphere, a 77 km thick whole slab model is constructed for simulation for the 2010 March 20 event (Fig. S7, Supporting Information). A structure of 70 km thick lithosphere underlying 7 km thick oceanic crust is placed below source. V_s and V_p in the lithosphere increase by 2 per cent and 1.5 per cent relative to the ambient mid-mantle, respectively. In the synthetic section, apart from the S700P resulting from the oceanic crust, another pronounced *SdP* arrival is shown right after S700P, which might be associated with the lithosphere structure. In addition, a strong arrival immediately ahead of S700P but with similar slowness compared to *P* is produced. Both of the later *SdP* and early prominent arrival are not observed in the data section. The significant discrepancy appears against the whole slab model. The simulation therefore suggests that oceanic crust perhaps partly detached from its underlying lithosphere before it descended into the lowermost mantle (D″ layer), likely as a result of interaction with 670 km discontinuity (Karato 1997) or other mechanisms like mechanical stirring throughout the deep mantle (Stixrude & Lithgow-Bertelloni 2012).

4.5 The fate of subducted oceanic crust

The existence of scatterers in mid-mantle is also confirmed by other seismic observations such as analyses of *ScS* reverberation data (Courtier & Revenaugh 2008) and investigations of PKP coda (Hedlin & Shearer 2002). The constrained depths ranging from ∼700 to 1110 km in this study exhibit excellent agreement with previous estimated values beneath various subduction zones (e.g. Kawakatsu & Niu 1994; Kaneshima & Helffrich 1999; Kaneshima 2003, 2009; Li & Yuen 2014), whereas only a few observations suggest presence of scatterers in the lower mid-mantle such as near 1600 km depth in Marianas region (Castle & van der Hilst 2003), suggesting separated crust is trapped substantially in the upper mid-mantle. This suggestion is additionally supported by the existence of water in the mid-mantle, inferred from observations of attenuation anomalies in the depths between ∼800 and 1100 km (e.g. Lawrence & Wysession 2006), and the water is most likely transported by subduction of voluminously hydrated slab. Note that many studies have suggested oceanic crust likely accumulated at a depth of ∼600 km (e.g. Shen & Blum 2003; Tauzin *et al.* 2013; Shen *et al.* 2014). This oceanic crust probably originated from stagnant slabs in the transition zone. All the observations together suggest that oceanic crust may be trapped substantially at the depths ranging from ∼600 to 1100 km. The later arrival *SdP* in this study is produced at one of many fragments of former separated oceanic crust in the mid-mantle with a favourable orientation (Fig. 4).

It has been postulated that subducted oceanic crust aggregates at the core-mantle boundary (CMB) to form thermochemical piles, explaining the cause of the large low shear velocity provinces (e.g. Hirose *et al.* 1999; Garnero 2000). However, a geodynamic simulation recently suggested that it is difficult for subducted oceanic crust to accumulate into large thermochemical piles near the CMB (Li & McNamara 2013). The reason for this scenario is due to intensively viscous stirring with ambient mantle, in particular associated with mantle plumes. Only a small amount of it may accumulate at

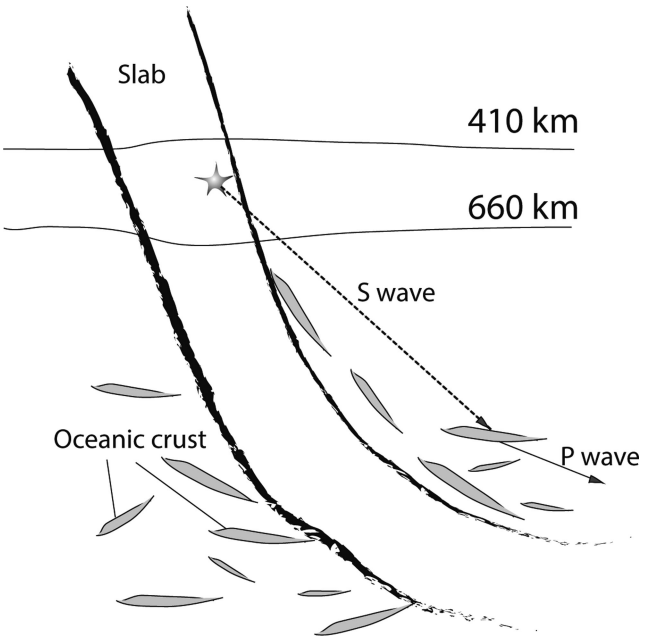

Figure 4. A schematic figure showing a slab trapped in the uppermost lower mantle (see more illustrations by Fukao & Obayashi 2013). The later arrival in this study is produced at one of many fragments of former oceanic crust with a favourable orientation.

the bases of plumes, but it is subsequently entrained away into the plume rather than accumulated (Li & McNamara 2013). Therefore, the issue whether the separated crust in the mid-mantle ultimately accumulated at the base of mantle may not be fully resolved until complete high-resolution images of slabs at various depths are successfully obtained.

5 CONCLUSION

In this study, we observe a clear later arrival in the NECESSArray recordings generated from four deep events beneath the west-central Pacific subduction zones. This second arrival is subsequently concluded to be an *S*-to-*P* conversion at a localized structure associated with past subducted oceanic crust below the sources by employing the array analysing techniques. The mid-mantle anomalous structures are characterized by MORB property attributed to subducted oceanic crust with a large depth variation (700–1110 km) in different subduction zones. This observation strongly favours the capability of the slabs penetrated into the lower mantle beneath some subduction zones, also indicates crustal component at least partly separates from the subducted oceanic lithosphere during various stages of subduction at great depths. Combined with other publications, we suggest that oceanic crust may be ubiquitously present in the mid-mantle of subduction zones, especially along the western Pacific subduction zones.

ACKNOWLEDGEMENTS

The authors gratefully acknowledge all the participants of the temporary seismic array (NECESSArray) in northeast China, and IRIS for making the array data available. The authors also thank three anonymous reviewers, together with the editor Jeannot Trampert and Andrea Morelli, for comments that significantly improved the manuscript. Figures were made with GMT (Wessel & Smith 1995) and GNUPLOT. This work was supported by the National Science Foundation of China (Grant No. 41330207) and the Fundamental Research Funds for the Central Universities (#2015QNA4041).

REFERENCES

Bentham, H. & Rost, S., 2014. Scattering beneath western Pacific subduction zones: evidence for oceanic crust in the mid-mantle, *Geophys. J. Int.,* **197,** 1627–1641.

Bonnardot, M.A., Régnier, M., Christova, C., Ruellan, E. & Tric, E., 2009. Seismological evidence for a slab detachment in the Tonga subduction zone, *Tectonophysics,* **464,** 84–99.

Brudzinski, M.R. & Chen, W.-P., 2005. Earthquakes and strain in subhorizontal slabs, *J. geophys. Res.,* **110,** B08303, doi:10.1029/2004JB003470.

Castle, J.C. & Creager, K.C., 1999. A steeply dipping discontinuity in the lower mantle beneath Izu–Bonin, *J. geophys. Res.,* **104**(B4), 7279–7292.

Castle, J.C. & van der Hilst, R.D., 2003. Searching for seismic scattering off mantle interfaces between 800 km and 2000 km depth, *J. geophys. Res.,* **108**(B2), 2095, doi:10.1029/2001JB000286.

Courtier, A.M. & Revenaugh, J., 2008. Slabs and shear wave reflectors in the midmantle, *J. geophys. Res.,* **113,** B08312, doi:10.1029/2007JB005261.

Fukao, Y. & Obayashi, M., 2013. Subducted slabs stagnant above, penetrating through, and trapped below the 660 km discontinuity, *J. geophys. Res.,* **118**(11), 5920–5938.

Garnero, E.J., 2000. Heterogeneity of the lowermost mantle, *Annu. Rev. Earth Planet. Sci.,* **28,** 509–537.

Grand, S.P., 2002. Mantle shear wave tomography and the fate of subducted slabs, *Phil. Trans. R. Soc. Lond., A,* **360,** 2475–2491.

Gudmundsson, O. & Sambridge, M., 1998. A regionalized upper mantle (RUM) seismic model, *J. geophys. Res.,* **103**(B4), 7121–7136.

Hall, R., 2002. Cenozoic geological and plate tectonic evolution of SE Asia and the SW Pacific: computer-based reconstructions, model and animations, *J. Asian Earth Sci.,* **20,** 353–434.

Hall, R. & Spakman, W., 2002. Subducted slabs beneath the eastern Indonesia–Tonga region: insights from tomography, *Earth planet. Sci. Lett.,* **201,** 321–336.

Hedlin, M.A.H. & Shearer, P.M., 2002. Probing mid-mantle heterogeneity using PKP coda waves, *Phys. Earth planet. Inter.,* **130,** 195–208.

Hedlin, M.A.H., Shearer, P.M. & Earle, P.S., 1997. Seismic evidence for small-scale heterogeneity throughout the Earth's mantle, *Nature,* **387,** 145–150.

Helffrich, G.R. & Wood, B.J., 2001. The Earth's mantle, *Nature,* **412,** 501–507.

Hirose, K., Fei, Y., Ma, Y. & Mao, H.-K., 1999. The fate of subducted basaltic crust in the Earth's lower mantle, *Nature,* **397,** 53–56.

Kaneshima, S., 2003. Small-scale heterogeneity at the top of the lower mantle around the Mariana slab, *Earth planet. Sci. Lett.,* **209,** 85–101.

Kaneshima, S., 2009. Seismic scatterers at the shallowest lower mantle beneath subducted slabs, *Earth planet. Sci. Lett.,* **286,** 304–315.

Kaneshima, S., 2013. Lower mantle seismic scatterers below the subducting Tonga slab: evidence for slab entrainment of transition zone materials, *Phys. Earth planet. Inter.,* **222,** 35–46.

Kaneshima, S. & Helffrich, G., 1999. Dipping low-velocity layer in the mid-lower mantle: evidence for geochemical heterogeneity, *Science,* **283**(5409), 1888–1892.

Karato, S.-i., 1997. On the separation of crustal component from subducted oceanic lithosphere near the 660 km discontinuity, *Phys. Earth planet. Inter.,* **99,** 103–111.

Kawakatsu, H. & Niu, F., 1994. Seismic evidence for a 920-km discontinuity in the mantle, *Nature,* **371,** 301–305.

Kennett, B.L.N. & Engdahl, E.R., 1991. Travel times for global earthquake location and phase identification, *Geophys. J. Int.,* **105,** 429–465.

Krüger, F., Baumann, M., Scherbaum, F. & Weber, M., 2001. Mid mantle scatterers near the Mariana slab detected with a double array method, *Geophys. Res. Lett.,* **28,** 667–670.

Lawrence, J.F. & Wysession, M.E., 2006. Seismic evidence for subduction-transported water in the lower mantle, in *Earth's Deep Water Cycle,* pp. 251–261, eds Jacobsen, S.D. & van der Lee, S., AGU Geophysical Monograph.

Li, M. & McNamara, A.K., 2013. The difficulty for subducted oceanic crust to accumulate at the Earth's core-mantle boundary, *J. geophys. Res.,* **118,** 1807–1816.

Li, J. & Yuen, D.A., 2014. Mid-mantle heterogeneities associated with Izanagi plate: implications for regional mantle viscosity, *Earth planet. Sci. Lett.,* **385,** 137–144.

Niu, F., 2014. Distinct compositional thin layers at mid-mantle depths beneath northeast China revealed by the USArray, *Earth planet. Sci. Lett.,* **402,** 305–312.

Niu, F. & Wen, L., 2001. Strong seismic scatterers near the core-mantle boundary west of Mexico, *Geophys. Res. Lett.,* **28,** 3557–3560.

Niu, F., Kawakatsu, H. & Fukao, Y., 2003. Seismic evidence for a chemical heterogeneity in the midmantle: a strong and slightly dipping seismic reflector beneath the Mariana subduction zone, *J. geophys. Res.,* **108,** 1978–2012.

Rost, S. & Thomas, C., 2002. Array seismology: methods and applications, *Rev. Geophys.,* **40**(3), 1008, doi:10.1029/2000RG000100.

Shang, X., Shim, S.-H., de Hoop, M. & van der Hilst, R., 2014. Multiple seismic reflectors in Earth's lowermost mantle, *Proc. Natl. Acad. Sci. USA,* **111**(7), 2442–2446.

Shen, Y. & Blum, J., 2003. Seismic evidence for accumulated oceanic crust above the 660-km discontinuity beneath southern Africa, *Geophys. Res. Lett.,* **30**(18), 1925, doi:10.1029/2003GL017991.

Shen, X., Yuan, X. & Li, X., 2014. A ubiquitous low-velocity layer at the base of the mantle transition zone, *Geophys. Res. Lett.,* **41,** 836–842.

Stixrude, L. & Lithgow-Bertelloni, C., 2012. Geophysics of chemical heterogeneity in the mantle, *Ann. Rev. Earth. planet. Sci.,* **40**(1), 569–595.

Tauzin, B., van der Hilst, R.D., Wittlinger, G. & Ricard, Y., 2013. Multiple transition zone seismic discontinuities and low velocity layer below western United States, *J. geophys. Res.,* **118,** 2307–2322.

Tsuchiya, T., 2011. Elasticity of subducted basaltic crust at the lower mantle pressures: insights on the nature of deep mantle heterogeneity, *Phys. Earth planet. Inter.,* **188,** 142–149.

van der Hilst, R., 1995. Complex morphology of subducted lithosphere in the mantle beneath the Tonga Trench, *Nature,* **374,** 154–157.

Vanacore, E., Niu, F. & Kawakatsu, H., 2006. Observations of the mid-mantle discontinuity beneath Indonesia from S to P converted waveforms, *Geophys. Res. Lett.,* **33,** L04302, doi:10.1029/2005GL025106.

Wang, R., 1999. A simple orthonormalization method for stable and efficient computation of Green's functions, *Bull. seism. Soc. Am.,* **89,** 733–741.

Wen, L. & Anderson, D.L., 1995. The fate of slabs inferred from seismic tomography and 130 million years of subduction, *Earth planet. Sci. Lett.,* **133**(1), 185–198.

Wessel, P. & Smith, W.H.F., 1995. New version of the generic mapping tools, *EOS, Trans. Am. geophys. Un.,* **76**(33), 329, doi:10.1029/95EO00198.

Zang, S.-X., Zhou, Y.-Z., Ning, J.-Y. & Wei, R.-Q., 2006. Multiple discontinuities near 660 km beneath Tonga area, *Geophys. Res. Lett.,* **33,** L20312, doi:10.1029/2006GL027262.

Zhou, Y.-Z., Yu, X.-W., Yang, H. & Zang, S.-X., 2012. Multiplicity of the 660-km discontinuity beneath the Izu-Bonin area, *Phys. Earth planet. Inter.,* **198,** 51–60.

SUPPORTING INFORMATION

Additional Supporting Information may be found in the online version of this paper:

Figure S1. Great circle paths (purple lines) link the four events (stars) with the seismic array (triangle) in northeast China. The corresponding piercing points at mid-mantle discontinuities are indicated as circles. Note that the true locations of seismic scatterers deviate from the great circle paths by certain degrees, which were estimated by beam-forming analyses (see Fig. 2).

Figure S2. Beam forming for four events data used in this study shows the first-arrival (*P*)'s slowness and backazimuth relative to the great circle.

Figure S3. (a) The seismic record section and (b) fourth root vespagram for the 2010 July 23 event. (c) The corresponding synthetic traces computed in a modified IASP91 model and (d) its vespagram. A scatterer at ∼910 km depth below the source is detected in the eastern Indonesia. Note that there may be some uncertainty in the estimated conversion depth and slowness due to complication in source time function of a great event.

Figure S4. (a) The seismic record section and (b) fourth root vespagram for the 2010 December 28 event. (c) The corresponding synthetic traces computed in a modified IASP91 model and (d) its vespagram. A scatterer at ∼780 km depth below the source is detected in Tonga region.

Figure S5. (a) The seismic record section and (b) fourth root vespagram for the 2011 February 21 event. (c) The corresponding synthetic traces computed in a modified IASP91 model and (d) its vespagram. Two scatterers at ∼780 and ∼1110 km depth below the source are detected in Tonga region. Note that an arrival at ∼75 s after *P* is partly visible in distances ranging from 88° to 90°. Further investigation is needed to clarify if this signal is produced by a scatterer at ∼1500 km depth. The slowness of S880P and S110P are not well predicted in the synthetic section, probably due to contamination of reverberations in between ∼780 and ∼1110 km depth.

Figure S6. (a) The synthetic section for the 2010 March 20 event, and the down-going *SV* waves have been filtered while modelling and (b) its vespagram. (c) A comparison of synthetic traces between filtering and no filtering. The synthetics clearly demonstrate that the later arrival has been removed after filtering, suggesting that the arrival is *S*-to-*P* not *P*-to-*P*.

Figure S7. (a) The seismic record section and (b) fourth root vespagram for the 2010 March 20 event. (c) The corresponding synthetic traces computed in a modified IASP91 model and (d) its vespagram. A 70 km thick lithosphere structure underlying a 7 km thick oceanic crust is placed below the source to conduct the waveform modelling. V_s and V_p in the lithosphere increase by 2 per cent and 1.5 per cent relative to the ambient mid-mantle, respectively. In the synthetic section, apart from the S700P relevant to the oceanic crust, another pronounced *SdP* arrival is also produced. In addition, a strong arrival immediately ahead of S700P but with similar slowness compared to *P* is predicted. The *SdP* and early prominent arrival are both not observed in the data section. And accordingly, we argue for a separation of crustal component from the slab, at least partly. (http://gji.oxfordjournals.org/lookup/suppl/doi:10.1093/gji/ggv314/-/DC1).

Please note: Oxford University Press is not responsible for the content or functionality of any supporting materials supplied by the authors. Any queries (other than missing material) should be directed to the corresponding author for the paper.